Article

JOURNAL OF COMPOSITE MATERIALS

Journal of Composite Materials
0(0) 1–19

DOI: 10.1177/0021998314568328
jcm.sagepub.com

SAGE

Effective properties evaluation for smart composite materials with imperfect fiber–matrix adhesion

Volnei Tita[1], Ricardo de Medeiros[1], Flávio D Marques[1] and Mariano E Moreno[2]

Abstract

A numerical approach is proposed to evaluate the effective properties of piezoelectric fibers embedded in a nonpiezoelectric matrix, considering imperfect contact between fiber and matrix. Firstly, a Representative Volume Element is analyzed via Finite Element Method for different loadings with suitable boundary conditions applied in a unique way. Transversely, isotropic piezoelectric materials with circular and square cross-section fibers are analyzed for square arrangements with different fiber volume fractions as well as with perfect and imperfect contact conditions. The results for circular and square cross-section fibers with perfect contact are compared to the literature data in order to verify the consistency of proposed numerical approach. After that, the results with imperfect contact are discussed, observing the influence of the fiber volume fraction and the level of the imperfection in the fiber–matrix adhesion. Results show that the imperfect contact not only influences the elastic constants, but also the piezoelectric effective values.

Keywords

Smart composite materials, effective properties, imperfect contact, active fiber composites, finite element analyses

Introduction

Smart composite materials present great potential for applications in aerospace industry as sensors and/or actuators for noise and vibration control, flow control, energy harvesting, and structural health monitoring (SHM). Regarding these applications, there are different types of smart composites, such as active fiber composite (AFC)[1] and macro fiber composite (MFC^{TM}).[2] These smart composites are made of piezoelectric materials (also denoted as PZT), which have the property of converting electrical energy into mechanical energy, and vice-versa. It is important to mention that either AFC or MFC consist on fibers of piezoelectric materials, which are embedded in a polymer matrix (conductive or not) polarized by electrodes (Figure 1(a) and (b)). Therefore, these smart composite materials show a high potential for application in engineering problems involving structural composite laminates, because they can be integrated in the structure as a single ply or reinforcements. Thus, problems involving piezoelectric materials (i.e. electromechanical coupling) have been investigated during last years. In fact, researchers have shown different approaches (analytical,[3–14] experimental,[15–17] and numerical[18–27]) to predict the mechanical, dielectric, and piezoelectric behavior of smart composite materials, which have been considered the perfect adhesion between fiber and matrix (perfect contact).

However, experimental results show that local or partial debonding in the interfaces is a rule rather than the exception in materials such as reinforced composites.[28] Thus, the existence of a rigid region is an idealization of the complex phenomenon, which occurs in the interface, where a transition zone (interphase) between the fiber and the matrix is omnipresent.

[1]Department of Aeronautical Engineering, São Carlos School of Engineering, University of São Paulo, Brazil
[2]Department of Mechanical Engineering, Center of Exact Sciences and Technology, Federal University of São Carlos, Brazil

Corresponding author:
Volnei Tita, Department of Aeronautical Engineering, São Carlos School of Engineering, University of São Paulo, Av. João Dagnone, 1100, 13573-120, São Carlos, SP, Brazil.
Email: voltita@sc.usp.br

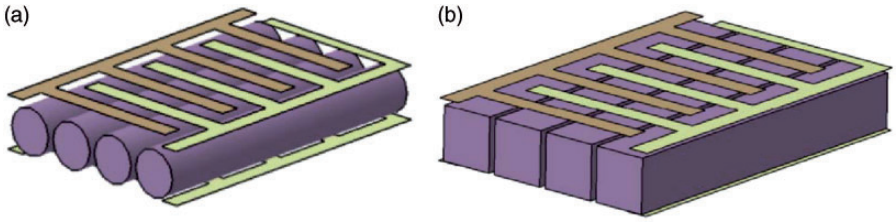

Figure 1. (a) AFC and (b) MFC^{TM} with electrodes.

This third phase may result from the manufacturing process (chemical treatments of fiber surfaces, resin crystallization and other effects) for the most fiber reinforced composites.[29] Although the thickness of interphase is small, this third phase plays a crucial role in the functionality and reliability of the composite materials and affects the overall mechanical properties of composites significantly. For instance, if the fiber–matrix adhesion is imperfect, then the continuity conditions for stresses and displacements are not satisfied. In fact, those phenomena[30–32] were shown in a model, where there is a bond between the reinforcements and the matrix, which is represented by an interphase with specified thickness and elastic properties different from those of the constituents. Then, in the interphase, stresses field is continuous, but displacements field is not. Caporale et al.[33] investigated the behavior of unidirectional fiber reinforced composites with imperfect interfacial bonding by the finite element method (FEM). In that work, an interfacial failure model was simulated by normal and tangential elastic springs, which connect the fiber nodes to the surrounded matrix nodes. Furthermore, Rodríguez-Ramos et al.,[34] López-Realpozo et al.,[35] and Sabina et al.[36] obtained a complete set of effective elastic moduli, considering a linear elastic composite material reinforced by parallel long circular fibers with a periodic arrangement. Also, an imperfect linear elastic fiber–matrix interphase was evaluated by the authors. More recently, Xu et al.[37] have predicted the effective elastic properties of long fiber reinforced composites, which had transversely isotropic material behavior by using a representative volume element (RVE). Hence, a model with three phases (fibers, matrix, and interphases between fibers and matrix) was applied to study the effects of the interphase on the effective elastic properties of composites. Rodríguez-Ramos et al.[38] presented the accuracy of different approaches, such as asymptotic homogenization method (AHM), semi-analytic method (SAM) and RVE solved by FEM, defined as FEM–RVE. All the models had imperfect contact for nonpiezoelectric materials.

In the literature, there are important scientific contributions about the determination of effective properties for smart composites, mainly with piezoceramic fibers embedded in a no-conductive matrix and imperfect contact for nonpiezoelectric materials. Observing those articles, based on numerical approaches, it is not common to find a detailed description of the models, how the boundary conditions are applied to obtain the effective properties, including imperfect contact condition. Considering this scenario, in this paper, finite element analyses are carried out for predicting the behavior of piezoelectric fibers (e.g. PZT) embedded in a nonpiezoelectric matrix (e.g. epoxy resin), regarding the influence of the imperfect contact. Thus, the effective properties for unidirectional periodic piezoelectric fiber composite, using individual properties of the constituent materials (fiber and matrix) and composite characteristics (e.g. geometry of the fiber, fiber volume fraction and imperfect contact) can be calculated. Thus, firstly, a RVE (unit cell) is analyzed via FEM for different loadings with suitable boundary conditions applied in a unique way, considering imperfect contact. After that, based on the theorem of average and on the numerical results, the effective properties are determined. This theory leads that the average mechanical, piezoelectric and dielectric properties of a unit cell are equal to the average properties of the composite material. For evaluating limitations and advantages of the proposed approach, different case studies are analyzed. Hence, transversely isotropic piezoelectric materials with circular and square cross-sectional fibers are investigated for square arrangements with different fiber volume fractions. The results for circular and square cross-section fibers with perfect contact are compared to the literature data in order to verify the consistency of the results obtained via proposed approach. And, the results for circular and square cross-section fibers with imperfect contact are discussed, observing the influence of the fiber volume fraction and the level of the imperfection in the fiber–matrix adhesion. It is very important to mention that these last results are the greatest novelty of the present paper.

Constitutive equations, Representative Volume Element (RVE), and imperfect condition

The constitutive equations for electro-mechanical behavior with piezoelectric coupling in smart composite

depend on the effective properties, which are evaluated in this work by using homogenization method taking into account a unit cell given by a RVE.

Constitutive equations for smart composite material

The elastic and the dielectric behaviors are coupled in piezoelectric materials, where the mechanical stress and strain variables are related to the electric field and displacement variables. The coupling between mechanical and electric fields is obtained by piezoelectric coefficients. The constitutive equations of piezoelectric materials are assumed linear and can be written in the following form

$$\begin{aligned} T_{ij} &= c^E_{ijkl}\, S_{kl} - e_{kij}\, E_k \\ D_i &= e_{ikl}\, S_{kl} + \varepsilon^S_{ik}\, E_k \end{aligned} \tag{1}$$

where T_{ij} and S_{ij} denotes the second rank stress and strain tensors, respectively, E_k and D_i are, respectively, the electric potential field and the electrical displacement vectors, c^E_{ijkl} denotes fourth-order elasticity tensor at constant electric field, e_{kij} is the third-order piezoelectric coupling tensor, and ε^S_{ik} is the second-order dielectric tensor at constant strain field.

Equation (1) can be written as a constitutive effective matrix format by Voigt's notation as

$$\begin{Bmatrix} \{T\} \\ \{D\} \end{Bmatrix} = \begin{bmatrix} [c]^E & -[e] \\ [e]^t & [\varepsilon]^S \end{bmatrix} \begin{Bmatrix} \{S\} \\ \{E\} \end{Bmatrix} \tag{2}$$

where the superscript t indicates transpose matrix, E constant electric field, and S constant strain field.

For an orthotropic (direction 3 aligned to the piezoelectric fibers) and transversely isotropic piezoelectric solid, the stiffness, the piezoelectric, and the dielectric matrices present 11 independent coefficients. Consequently, the constitutive relations in equation (2) can be written in terms of the following expanded matrix form

$$\begin{Bmatrix} T_{11} \\ T_{22} \\ T_{33} \\ T_{12} \\ T_{23} \\ T_{31} \\ D_1 \\ D_2 \\ D_3 \end{Bmatrix} = \begin{bmatrix} c^E_{11} & c^E_{12} & c^E_{13} & 0 & 0 & 0 & 0 & 0 & -e_{13} \\ c^E_{13} & c^E_{11} & c^E_{13} & 0 & 0 & 0 & 0 & 0 & -e_{13} \\ c^E_{13} & c^E_{13} & c^E_{33} & 0 & 0 & 0 & 0 & 0 & -e_{33} \\ 0 & 0 & 0 & c^E_{66} & 0 & 0 & 0 & 0 & 0 \\ 0 & 0 & 0 & 0 & c^E_{44} & 0 & 0 & -e_{15} & 0 \\ 0 & 0 & 0 & 0 & 0 & c^E_{44} & -e_{15} & 0 & 0 \\ 0 & 0 & 0 & 0 & 0 & e_{15} & \varepsilon^S_{11} & 0 & 0 \\ 0 & 0 & 0 & 0 & e_{15} & 0 & 0 & \varepsilon^S_{11} & 0 \\ e_{13} & e_{13} & e_{33} & 0 & 0 & 0 & 0 & 0 & \varepsilon^S_{33} \end{bmatrix} \begin{Bmatrix} S_{11} \\ S_{22} \\ S_{33} \\ S_{12} \\ S_{23} \\ S_{31} \\ E_1 \\ E_2 \\ E_3 \end{Bmatrix} \tag{3}$$

The smart composites effective properties can be defined by the average fields in the same form as equation (2), which can be written in a compact matrix form

$$\begin{Bmatrix} \{\bar{T}\} \\ \{\bar{D}\} \end{Bmatrix} = \begin{bmatrix} [c]^E_{eff} & -[e]_{eff} \\ [e]^T_{eff} & [\varepsilon]^S_{eff} \end{bmatrix} \begin{Bmatrix} \{\bar{S}\} \\ \{\bar{E}\} \end{Bmatrix} \tag{4}$$

where the subscript *eff* denotes effective property.

The homogenization approach for composite materials refers to find a functional dependence between the average variables of the material model, which can represent the coherent physical behavior. Based on the theorem of average with a homogenized model, mechanical and electrical properties of a unit cell, or RVE, are taken from average properties of the composite material. It is assumed that the average mechanical and electrical properties of a unit cell are equal to the average properties of the composite material as follows

$$\langle T_{ij} \rangle = \overline{T}_{ij}, \quad \langle D_k \rangle = \overline{D}_k, \quad \langle S_{ij} \rangle = \overline{S}_{ij}, \quad \langle E_k \rangle = \overline{E}_k \tag{5}$$

The average stresses, strains, electric fields, and electrical displacements in the RVE are defined by

$$\begin{aligned} \overline{T}_{ij} &= \frac{1}{|V|}\int_{|V} T^0_{ij}\mathrm{d}V, \quad \overline{S}_{ij} = \frac{1}{|V|}\int_V S^0_{ij}\mathrm{d}V \\ \overline{D}_i &= \frac{1}{|V|}\int_V D^0_i\mathrm{d}V, \quad \overline{E}_i = \frac{1}{|V|}\int_V E^0_i\mathrm{d}V \end{aligned} \tag{6}$$

where $|V|$ is the unit cell volume and $\overline{T}_{ij}$, $\overline{S}_{ij}$, $\overline{D}_i$, and $\overline{E}_i$ denote stress, electrical displacement, strain, and electric potential average values, respectively.

Using the FEM, the average values can be calculated by

$$\begin{aligned} \overline{T}_{ij} &= \frac{1}{V}\sum_{n=1}^{nel} T^{(n)}_{ij} V^{(n)}, \quad \overline{S}_{ij} = \frac{1}{V}\sum_{n=1}^{nel} S^{(n)}_{ij} V^{(n)} \\ \overline{D}_i &= \frac{1}{V}\sum_{n=1}^{nel} D^{(n)}_i V^{(n)}, \quad \overline{E}_i = \frac{1}{V}\sum_{n=1}^{nel} E^{(n)}_i V^{(n)} \end{aligned} \tag{7}$$

where $|V|$ is the volume of the unit cell, *nel* is the number of elements of the complete unit cell, $V^{(n)}$ is the volume of the nth element, and $T_{ij}^{(n)}$, $S_{ij}^{(n)}$, $D_i^{(n)}$, and $E_i^{(n)}$ are the respective tensors evaluated in the nth element.

Representative volume element (RVE)

In this work, the RVE is assumed as combinations of piezoelectric fibers embedded in a polymer matrix, including an interface, obeying a specified fiber volume fraction. This RVE is modeled by solid finite elements. Thus, the numerical model is used to determine a homogeneous medium equivalent to the original composite and comprises the smallest portion of the smart composite, which keeps the most representative combination of its main materials. It is important to notice that several types of fibers arrangements can be used, as discussed by Kar-Gupta and Venkatesh.[21] Figure 2 illustrates a unit cell, considering square arrangement of fibers in the composite material. This unit cell can represent the behavior of smart composite material as a whole, assuming that it has infinite length (or much larger than the diameter of fiber) in the three orthotropic directions, since suitable symmetry conditions are imposed in the RVE model. Thus, this hypothesis requires that the material has the same properties in both directions normal to the length of the fiber (directions 1 and 2, Figure 2). In order to attend this requirement, transversal isotropy is adopted in the present work.

Knowing the material properties of each constituent and through combinations of loads and appropriate boundary conditions, it is possible to obtain the constitutive matrix parameters. Whereas the smart composite is made of composite piezoelectric stacked in layers (multilayer), and the polarization could occur between each layer or between the outer faces of the laminate. It is important to notice that the present approach can be extended to other types of smart composites, for instance, materials with only a single layer, such as MFC™.

In Figure 3, it can be observed details of the circular cross-section RVE (square arrangement), including the representation for each of the cube faces (denoted as X^+, X^-, Y^+, Y^-, Z^+, and Z^-) and the local reference system (1-2-3). It is worth to mention that for all further analyses, the piezoelectric fibers are considered continuous and orientated to the z-axis (or in direction 3). In addition, as commented earlier, the unit cell shows three phases: matrix, fiber, and interphase (Figure 3).

The spatial periodicity in a RVE demands compatibility conditions with respect to the opposite edges in the faces shown by Figure 3. Adjacent RVEs must have identical deformations, while neither overlapping nor separation may occur. Considering composite materials as a periodical array of unit cells, the periodical boundary conditions described by Jin et al.[39] and Xia et al.[40] must be applied to ensure the repeatability of the RVE. Moreover, this compatibility condition is used to avoid separation or overlap between the neighboring RVE and it is defined as condition of parallelism given by

$$u_i^{+j} - u_i^{-j} = c_i^j (i, j = x, y, z) \tag{8}$$

where u_i^j denotes the displacement along the i-direction of one node located at the boundary face whose normal vector is along the j-direction. The plus sign in superscript means the normal vector of the boundary face, which is in positive j-direction, while the minus sign means the opposite.

Actually, u_i^{+j} and u_i^{-j} are displacements of one pair of nodes at opposite boundary faces, with identical coordinates in the other two directions except the j-direction. The parameter c_i^j is constant, so all node

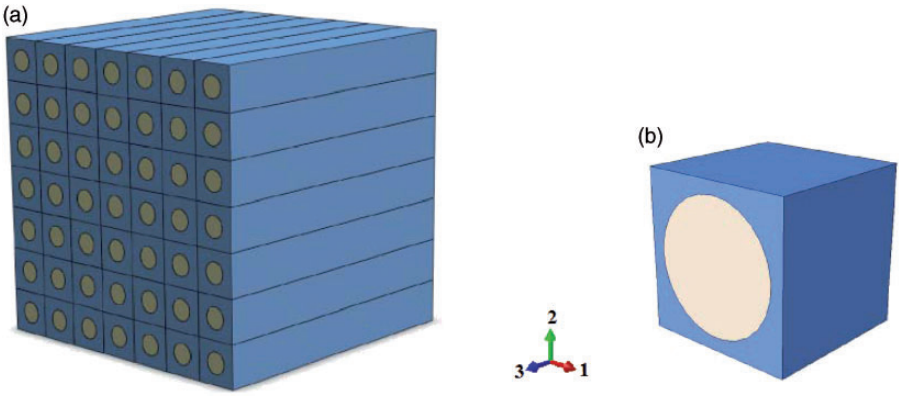

Figure 2. (a) Composite with unidirectional fibers in square arrangement; (b) correspondent unit cell.

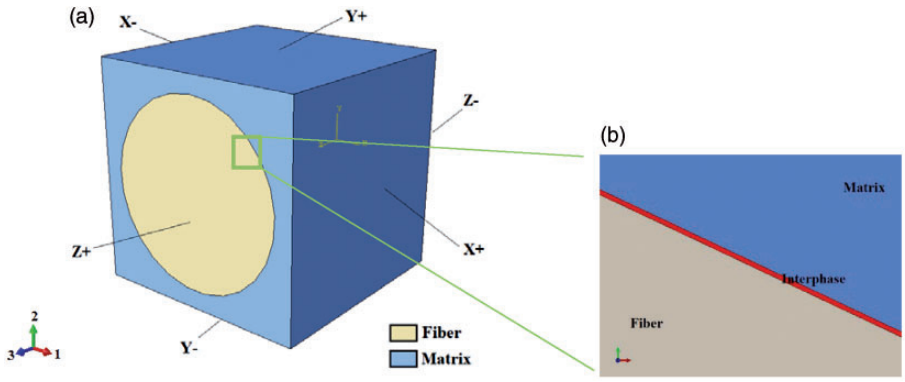

Figure 3. (a) Notation for different surfaces of the unit cell and (b) three phases in details.

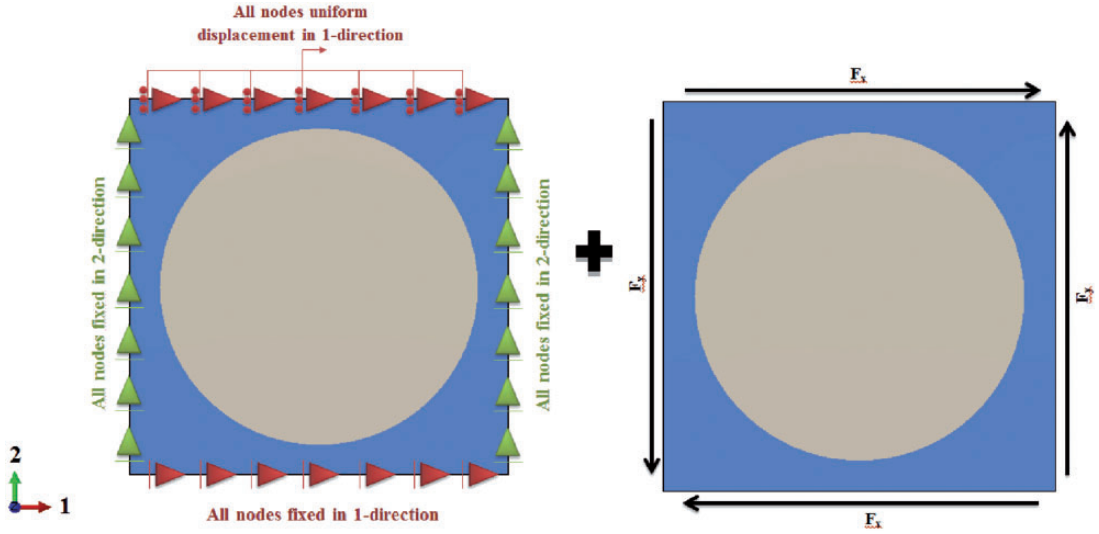

Figure 4. Illustration of periodical boundary conditions for 1-2 longitudinal shear loading (symmetric BCs for direction 3).

pairs defined in equation (8) have the same difference of displacement in the *i*-direction.[40] Figure 4 shows a schematic illustration of these periodical boundary conditions under transversal tensile and longitudinal shear loadings. In fact, for the proposed approach, it is not necessary to specify these conditions for some loading cases, where the displacement and electrical boundary conditions already ensure the parallelism restriction. Automatic procedures to search opposite nodes and applying restrictions are used by the implementation of subroutines in Python language to avoid selection errors of node pairs.

Imperfect fiber–matrix adhesion

Regarding fiber-reinforced composite, it is important to mention that the micromechanical models can be applied to determine the response of fiber reinforced composites with perfect fiber–matrix adhesion (perfect contact) as function only of the fiber and the matrix behaviors. However, for imperfect contact fiber–matrix, it is necessary to evaluate the influence of the interface. In this present work, the hypothesis that there are no discontinuities in the physical model was assumed. The interphase degraded physically or chemically is simulated by a set of element with degraded properties. Thus, the interphase properties are considered isotropic and calculated by

$$\begin{aligned} C_{11} &= C_{22} = C_{33} = \lambda + 2\mu \\ C_{12} &= C_{23} = C_{13} = \lambda \\ C_{44} &= C_{55} = C_{66} = \mu = \frac{(C_{11} - C_{12})}{2} \\ \lambda &= t(K_n - 2K_t) \\ \mu &= G = tK_t \end{aligned} \tag{9}$$

as a consequence of the formulation provided by Hashin,[32] where K_n and K_t are spring constants per unit of area (i.e. material parameters) and t is the thickness of

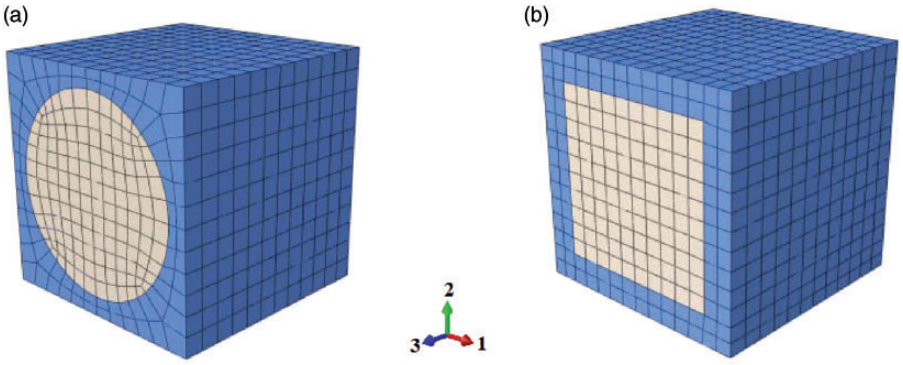

Figure 5. Square arrangement with: (a) circular and (b) square cross sections.

the interphase. It is important to highlight that K_n is related to normal direction contact behavior and K_t is related to tangential direction contact behavior. Other formulations show another parameter for tangential direction contact behavior defined as K_s, but in the present work, where the interface is modeled as isotropic material, the values for K_t and K_s will be assumed equal as implicitly shown by equation (9). Moreover, the thickness of interphase can be calculated in function of the dimension of the fiber, for example "a" is equal the radius for circular fiber multiplied by a factor η.[32] In this work, for the proposed RVE, the radius for circular and the edge for square cross-section fibers are variable according to the fiber volume fraction to be investigated, but the edge of the cube is constant. In addition, the cube has volume equal 1.0 mm^3 and the ratio between the fiber radius and thickness of the interphase is constant and equal to 0.001 ($t/a = 0.001$) in all analyses.

Different case studies can be investigated, considering not only perfect contact, i.e. $K_n, K_t \to \infty$, but also complete decohesion of the piezoelectric fibers, i.e. $K_n, K_t \to 0$, as well as different levels of mechanical imperfections between fiber and matrix. Therefore, the simulation of the imperfect interface was modeled by degraded the properties of the interphase, and contact algorithms were not used as approached by other authors. Thus, the proposed RVE has conventional connections between the nodes of the finite element mesh. In addition, for numerical analyses of the perfect contact, finite values of stiffness constants K were arbitrarily defined equal to 1×10^{10} ($N/mm \times mm^{-2}$).

Effective properties evaluation via finite element analysis

Different case studies were investigated in order to determine the effective properties via finite element analysis (FEA). Therefore, RVE transversely isotropic finite element models with square arrangement, showing perfect or imperfect contact conditions, were developed and analyzed.

Circular and square cross-section piezoelectric fibers: RVE models

Square arrangement is applied for circular and square cross sections as shown by Figure 5. In the FEA carried out by using Abaqus™ version 6.10,[42] as commented earlier, the cube has volume equaling 1.0 mm^3 and the ratio between the fiber radius and thickness of the interphase is constant and equal to 0.001 in all analyses. For real PZT fibers, the square cross sections are not perfectly square or circular, but all models[15–27] presented this hypothesis. Different fiber volume fractions from 10% to 70% are imposed in the unit cell (Figure 6). For meshing the unit cell three-dimensional multi-field 20-node elements are used. These quadratic piezoelectric brick elements (C3D20E – Abaqus™ nomenclature for the element[42]) have three mechanical displacement degrees of freedom (DOF) and an additional electric potential DOF. Thus, it is possible to perform fully coupled electromechanical analyses.

Material properties

The smart composite material is made of circular or square piezoceramic fiber (PZT-5 A) and epoxy matrix is separated by an interphase. The material properties of the epoxy resin and piezoelectric fiber are taken from Berger et al.[19] as shown in Table 1, according to orthotropic directions (1, 2, and 3).

Loadings and boundary conditions applied on the RVE models

The simplified set of constitutive equations (cf. equation (2)), with prescribed boundary conditions allow the evaluation of the effective material properties. Owing to the boundary conditions applied in the RVE, more than one coefficient is obtained for each

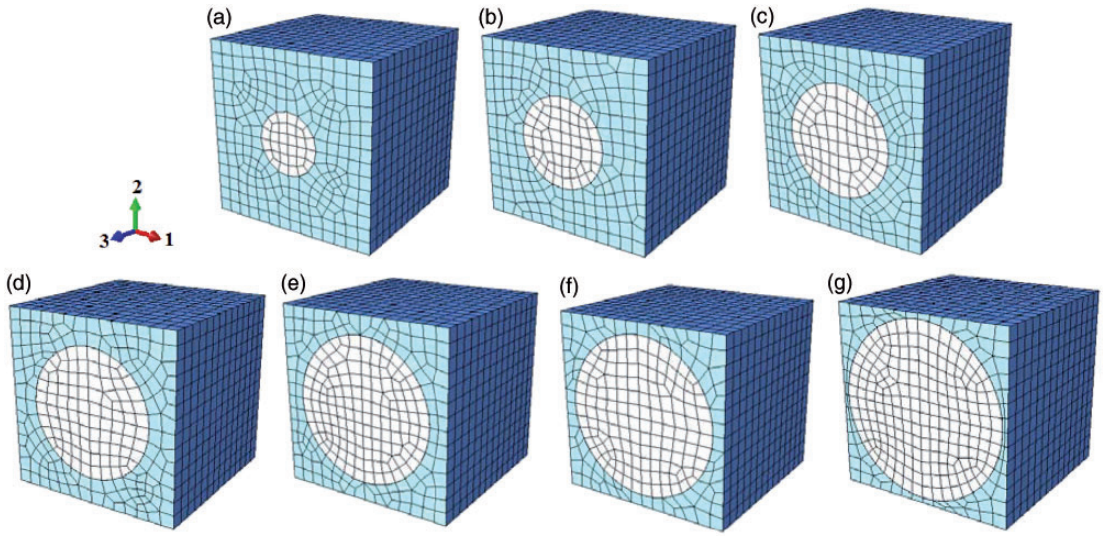

Figure 6. Circular fiber with fiber volumetric fraction equal to: (a) 10%; (b) 20%; (c) 30%; (d) 40%; (e) 50%; (f) 60%; (g) 70%.

Table 1. Material properties for fiber (piezoceramic) and matrix (resin epoxy).[19]

	C_{11}	C_{12}	C_{13}	C_{33}	C_{44}	C_{66}	e_{13}	e_{15}	e_{33}	ε_{11}	ε_{33}
	GPa						C/m^2			nF/m	
Fiber	121.0	75.4	75.2	111.0	21.1	22.8	−5.4	12.3	15.8	8.11	7.35
Matrix	3.86	2.57	2.57	3.86	0.64	0.64	–	–	–	0.0797	0.0797

analysis. Therefore, to evaluate all 11 effective coefficients, only six analyses are necessary. More accurate results are obtained when loading is applied in fiber longitudinal direction, denoted here as z-direction (or direction 3), as well as x-direction and y-direction, which are aligned with directions 1 and 2, respectively. Table 2 shows the summarized boundary conditions and loadings used in this work.

The first and second analyses involve the loading applied in z-direction (fiber direction), the first one with mechanical loading and the second one with electrical loading. The applied boundary conditions already ensure the parallelism conditions; so they do not need to be specified again by constraint equations. Third and fourth analyses are similar to the first set, but the mechanical and electrical loadings are applied in x-direction. Again, the constraint equations are already ensured by the boundary conditions.

However, the last two analyses related earlier involve the RVE subjected to shear loading. In the fifth analysis, the shear loading is performed in plane x-y and in the sixth, in plane y-z. Both cases require explicit implementation of constraining equations. The implementation is done by using Abaqus™ with Python Language due the direct access to the model data. It is also necessary to include some notes about other procedures adopted to impose the analysis conditions in numerical simulations for the fifth and sixth analyses:

1. When applying constraint equations between opposite unit cell faces, nodes that belong to the unit cell edges perpendicular to the shearing plane should not be included. For example, for x-y shear loading, the edge nodes are disregarded (red lines in Figure 7).
2. When applying the shear forces, the loading should be distributed along face nodes, except those indicated by the red lines in Figure 7. Therefore, it is a procedure similar that was adopted for the constraint equations. For the y-z shear case, analogous recommendations must be followed, considering the nodes at the edges aligned with x-axis highlighted in red.

In addition, for numerical analyses, it was investigated the influence of the mesh density. Thus, three different meshes were used. Firstly, to evaluate the effective coefficients, RVE was meshed by using approximately 4000 elements. After that, 8000, 12,000, and 16,000 elements were used. However, the results showed that the differences for the effective coefficients are of 10^{-4} order, considering the used mesh densities. Therefore, all the results are shown only for

Table 2. Loadings and boundary conditions (BCs).

	Equation[a]	Prescribed displacement field (m)	Prescribed force field (N)	Prescribed electric potential field (V)	Displacement BCs (m)	Electric potential BCs (V)
1st line	$c_{13}^{eff} = \frac{\bar{T}_{11}}{\bar{S}_{33}} c_{33}^{eff} = \frac{\bar{T}_{33}}{\bar{S}_{33}}$	Positive u_Z surface Z^+	–	–	Zero normal displacements surfaces X^+, X^-, Y^+, Y^-, Z^-	Zero all surfaces
3rd line					$S_{11} = S_{22} = S_{12} = S_{23} = S_{31} = 0$	$E_1 = E_2 = E_3 = 0$
1st line	$e_{13}^{eff} = \frac{\bar{T}_{11}}{\bar{E}_3}$	–	–	Positive voltage surface Z^+	Zero normal displacements all surfaces $S_{11} = S_{22} = S_{33} = S_{12} = S_{23} = S_{31} = 0$	Zero surface Z
3rd line	$e_{33}^{eff} = -\frac{\bar{T}_{33}}{\bar{E}_3}$					
9th line	$\varepsilon_{33}^{eff} = \frac{\bar{D}_3}{\bar{E}_3}$					
1st line	$c_{11}^{eff} = \frac{\bar{T}_{11}}{\bar{S}_{11}}$	Positive u_X surface X^+	–	–	Zero normal displacements surfaces X-, Y^+, Y^-, Z^+, Z^-	Zero all surfaces
2nd line	$c_{12}^{eff} = \frac{\bar{T}_{22}}{\bar{S}_{11}}$				$S_{22} = S_{33} = S_{12} = S_{23} = S_{31} = 0$	$E_1 = E_2 = E_3 = 0$
7th line	$\varepsilon_{11}^{eff} = \frac{\bar{D}_1}{\bar{E}_1}$	–	–	Positive voltage surface X^+	Zero normal displacements all surfaces $S_{11} = S_{22} = S_{33} = S_{12} = S_{23} = S_{31} = 0$	Zero surface X^-
4th line	$c_{66}^{eff} = \frac{\bar{T}_{12}}{\bar{S}_{12}}$	–	$+F_y$ and $-F_y$ surfaces X^+ and X^- $+F_x$ and $-F_x$ surfaces Y^+ and Y^-	–	Zero y-displacements faces X^+, X^- Zero x-displacements surface Y^- Uniform x-displacements surface Y^+	Zero all surfaces
5th line	$e_{15}^{eff} = \frac{(-\bar{E}_2 \cdot \varepsilon_{11} + \bar{D}_2)}{\bar{S}_{23}}$	–	$+F_y$ and $-F_y$ surfaces Z^+ and Z^-	–	Zero y-displacements surfaces Z^+, Z^- Zero z-displacements surface Y^- Uniform z-displacements surface Y^+	Zero surfaces X^+, X^-, Y^+, Y^-
8th line	$c_{44}^{eff} = \frac{\left(\bar{T}_{23} + \bar{E}_2 \cdot e_{15}^{eff}\right)}{\bar{S}_{23}}$		$+F_z$ and $-F_z$ surfaces Y^+ and Y^-			

[a]Lines number referred to equation (3).

the meshed RVE by using approximately 4000 elements. It is worth highlighting that Abaqus™ calculates the quantities for the tensors in Gauss points, and it uses numerical techniques to integrate various quantities over the volume of each element in order to feed equation (7). Also, the element type C3D20E has 27 integration points.

Results and discussion

Initially, it was calculated the effective coefficients for a smart composite material with piezoelectric circular and square cross-section fiber, epoxy resin matrix and perfect fiber–matrix adhesion (perfect contact). As observed in Figures 8 and 9, it is possible to assess the numerical results via RVE in order to calculate the parameters required by equation (3).

In order to compare to the literature data,[19] all 11 effective coefficients (equation (3)) were calculated for one specific fiber volume fraction (55.5%) and circular cross-section fiber. Thus, the proposed approach was applied and the results were compared to analytical results obtained via AHM as shown in Table 3.

Observing Table 3, by one side, major differences (Δ) between analytical and numerical proposed

approach are c_{11}^{eff}, c_{12}^{eff}, c_{66}^{eff}, and e_{15}^{eff}. Similarly, other authors[19–27] also stated these differences for those coefficients. In fact, some coefficients are mainly influenced by the composite behavior in the plane 1-2. It is important to notice that for square arrangement and loads applied on the plane 1-2, periodical boundary conditions for 1-2 longitudinal shear loading were only applied on the matrix part of the RVE (see Figure 4). However, in direction 3, the boundary conditions were applied not only on the matrix, but also in the other constituents (interphase and fiber). This is one reason that can explain the difference of the effective coefficient in the plane 1-2. Moreover, the RVE model is highly influenced by the applied boundary conditions, because the values involved in the equations are concomitantly in Giga and Nano order. By other side, for the remaining effective coefficients, mainly aligned to direction 3, the proposed approach has shown good agreement with those presented by AHM.[19]

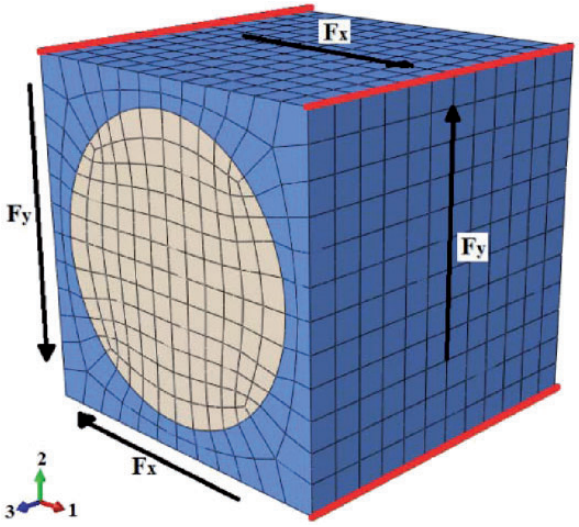

Figure 7. Edge nodes without forces and boundary conditions for shear loading.

In the literature, it is possible to find different universal relations like provided by Guinovart-Diaz et al.,[41] which is developed for three-phase composites. However, in order to verify the accuracy of the present model with perfect contact (i.e. similar to two-phase composites), the theory developed by Benveniste and Dvorak was used.[6] This theory was based on the central idea of the creation of uniform fields in heterogeneous media by proper boundary conditions. Relations that can be used to determine the effective properties of piezoelectric composite are presented, which was called Universal Relations. It is important to mention that relations were presented for different piezoelectric classes. In this work, the tetragonal crystal class 4 mm was considered, i.e. transversely isotropic piezoelectric composites. The equations were given by

$$\frac{k - v_f k_f - v_m k_m}{l - v_f l_f - v_m l_m} = \frac{l - v_f l_f - v_m l_m}{n - v_f n_f - v_m n_m} = \frac{j - v_f j_f - v_m j_m}{g - v_f g_f - v_m g_m} = \frac{k_f - k_m}{l_f - l_m} \tag{10}$$

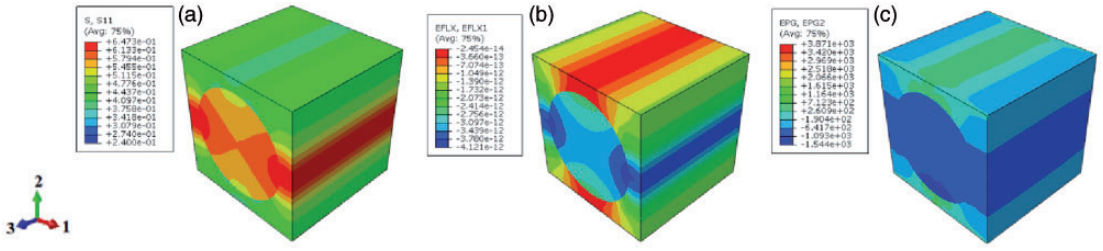

Figure 8. Circular fiber with perfect contact ($K_n = K_t = \infty$): (a) first analysis T_{11}; (b) fourth analysis D_1; (c) sixth analysis E_2.

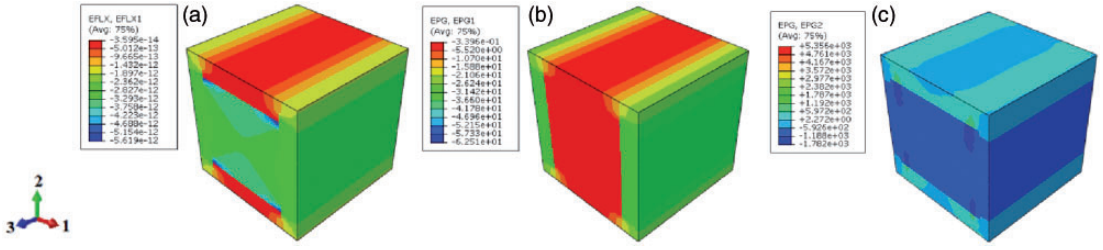

Figure 9. Square fiber with perfect contact ($K_n = K_t = \infty$): (a) fourth analysis D_1; (b) fourth analysis E_1; (c) sixth analysis E_2.

Table 3. Effective properties of circular cross section for square arrangements and perfect contact.

Units	c_{11}^{eff}	c_{12}^{eff}	c_{13}^{eff}	c_{33}^{eff}	c_{44}^{eff}	c_{66}^{eff}	e_{13}^{eff}	e_{15}^{eff}	e_{33}^{eff}	ε_{11}^{eff}	ε_{33}^{eff}
	GPa							C/m^2		nF/m	
(1)	9.7394	5.5898	6.0792	35.0707	2.1462	2.0853	−0.2496	0.0221	10.8611	0.2778	4.2088
(2)	10.8560	4.6656	6.0434	35.1268	2.2050	1.5277	−0.2584	0.0250	10.8642	0.2867	4.2704
Δ(%)	11.46	16.53	0.59	0.16	2.74	26.74	3.53	13.12	0.03	3.20	1.46

Δ – Comparison between (1) Berger et al.[19] and (2) present work.

Table 4. Universal Relations[6] applied in order to determine the accuracy of the present work by square arrangement.

	Eq. $(10)_1$ F_1	Eq. $(10)_2$ F_2	Eq. $(10)_3$ F_3	Eq. $(10)_4$ F_4	Eq. $(11)_1$ F_5	Eq. $(11)_2$ F_6	Eq. $(11)_{13}$ F_7	Eq. $(11)_4$ F_8	Eq. (12) F_9
(1)	1.3116	1.3026	1.3132	1.3078	–	–	–	–	–
(2)	1.3077	1.3064	1.3071	1.3078	–	–	–	–	–
(1)	–	–	–	–	−7.4657E−11	−7.4051E−11	−4.4971E−11	−7.4349E−11	–
(2)	–	–	–	–	−7.4345E−11	−7.4309E−11	−7.4305E−11	−7.4349E−11	–
(1)	–	–	–	–	–	–	–	–	5.3573E−3
(2)	–	–	–	–	–	–	–	–	7.6006E−3

(1) Berger et al.[19]
(2) Present work.

Table 5. Comparison between the results provided by the numerical approach and the Universal Relations.

	$\Delta(F_1)$–(F_2)	$\Delta(F_1)$–(F_3)	$\Delta(F_1)$–(F_4)	$\Delta(F_2)$–(F_3)	$\Delta(F_2)$–(F_4)	$\Delta(F_3)$–(F_4)
(1)	0.687%	0.125%	0.289%	0.817%	0.400%	0.414%
(2)	0.097%	0.047%	0.007%	0.049%	0.104%	0.054%
	$\Delta(F_5)$–(F_6)	$\Delta(F_5)$–(F_7)	$\Delta(F_5)$–(F_8)	$\Delta(F_6)$–(F_7)	$\Delta(F_6)$–(F_8)	$\Delta(F_7)$–(F_8)
(1)	0.811%	39.763%	0.412%	39.271%	0.402%	65.328%
(2)	0.049%	0.054%	0.006%	0.005%	0.055%	0.060%

$\Delta = [|(a_n)\text{-}(a_n+1)|/((a_n+a_{n+1})/2)] \times 100$.
(1) Berger et al.[19]
(2) Present work.

$$\frac{j - v_f j_f - v_m j_m}{l - v_f l_f - v_m l_m} = \frac{g - v_f g_f - v_m g_m}{n - v_f n_f - v_m n_m} = \frac{-q + v_f q_f + v_m q_m}{g - v_f g_f - v_m g_m} = \frac{j_f - j_m}{l_f - l_m} \tag{11}$$

$$\det \begin{bmatrix} c_{44}^{eff} & \varepsilon_{11}^{eff} & e_{15}^{eff} \\ G_L^f & t_f & h_f \\ G_L^m & t_m & h_m \end{bmatrix} = 0 \tag{12}$$

where the subscripts f and m denote fiber and matrix, respectively. Also, $k = (c_{11}^{eff} + c_{12}^{eff})/2$, $c_{13}^{eff} = l$, $c_{33}^{eff} = n$, $e_{13}^{eff} = j$, $e_{33}^{eff} = g$, $e_{15}^{eff} = h$, $\varepsilon_{11}^{eff} = t$, and $\varepsilon_{33}^{eff} = q$ were considered.

Table 4 presents the result of these relations by using the effective properties determined in this work and given by Berger et al.[19] Table 5 shows the relative differences between the results presented in the Table 4. Some differences can be explained due to the method used by the present authors to extract results published by Berger et al.[19] in figure format. It is possible to see that the effective properties determined in this work have more accuracy than the properties given by AHM.[19] These differences for the present work are smaller than 0.1%.

Several hypotheses can be adopted to illustrate the crystal symmetry, creating a variety of combinations for the matrix and fiber with different degree of anisotropy. In this study, it was adopted that the piezoelectric fibers and the matrix were transversely isotropic. Consequently, the result for this combination leads to a transversely isotropic behavior for the RVE. Based on the universal relations and using the effective

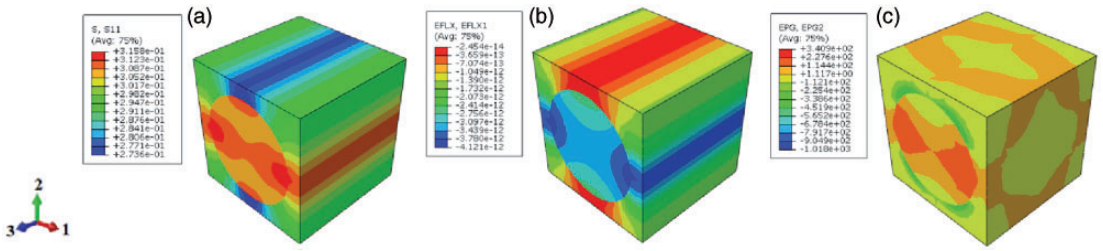

Figure 10. Circular fiber with imperfect contact ($K_n = \infty$ and $K_t = 1$): (a) first analysis T_{11}; (b) fourth analysis D_1; (c) sixth analysis E_2.

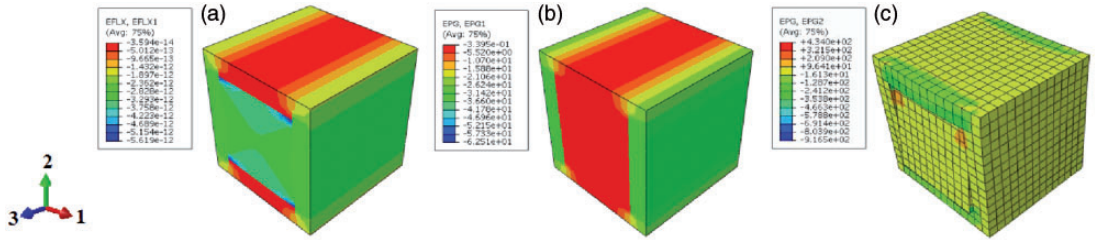

Figure 11. Square fiber with imperfect contact ($K_n = \infty$ and $K_t = 1$): (a) fourth analysis D_1; (b) fourth analysis E_1; (c) sixth analysis E_2.

properties for hexagonal arrangement given by Medeiros et al.,[24] it was possible to verify that the square arrangement has higher accuracy. This can be explained because the crystal system 4 mm for the square arrangement.

After the evaluations of smart composite materials with circular cross-section fibers, considering perfect contact for a specified fiber volume fraction, other case studies were investigated. For those case studies, it was evaluated not only the influence of different levels for imperfections in the fiber–matrix adhesion, but also different fiber volume fractions and different geometries for the fiber cross section. Figures 10 and 11 show the finite element results for piezoelectric circular and square cross-section fibers, respectively, with epoxy resin matrix, considering imperfections in the fiber–matrix adhesion.

In Figures 12 to 22, there are the results for all effective coefficients calculated by the numerical proposed approach, considering square arrangement, circular and square cross sections, and different contact conditions, i.e. K_n equal to ∞ (hard contact hypothesis between fiber and matrix for normal direction was assumed) and K_t equal to 1×10^0, 1×10^5, and 1×10^{10} (N/mm $\times$ mm^{-2}).

Furthermore, there are comparisons among the results for circular and square cross sections to the uniform field method (UFM), given by Nan and Jin,[7] considering different fiber volume fractions. In fact, Nan and Jin[7] showed a general theory for predicting the effective properties of piezoelectric composites with square fiber, defined as UFM. This approach is based on the iso-fields assumption such that stresses, strains, electric field. and electric displacements are uniform throughout the structure for the macroscopic level. Thus, the UFM neglects the micro-structural details.

Figures 12 and 13 show the effective coefficients associated to directions 1 and 2 (transverse direction). These coefficients exhibit higher differences, considering different level of properties degradation, mainly for fiber volume fractions higher than 30%. In fact, these differences can be more than 100%. Thus, it is observed that for values of K_t equal to 10^5 and 10^{10}, there were not large differences in the response for low fiber volume fraction. However, if volume fractions are increased, then the differences are also increased. Although the cube dimensions are equal for all analyses, because only the fiber dimension in the RVE changes, it is very important to notice that the contact area between the fiber and the matrix increases, when the fiber volume fraction increases. Therefore, the influence of the K_t is important, but the contact area is also relevant for the calculation of the effective properties of smart composites. This explains why the differences increase for K_t equal 10^5 and 10^{10}, when the fiber volume fractions increase.

Figures 14 and 15 show the effective coefficients associated to directions 1 and 3 (transverse and longitudinal directions, respectively). It can be noticed that only the transverse direction presents variation in the effective properties. These differences can be also higher than 100% when different levels of imperfection were considered.

Regarding Figures 16 and 17, it is possible to observe that the effective values for K_t equaling 1×10^0 (N/

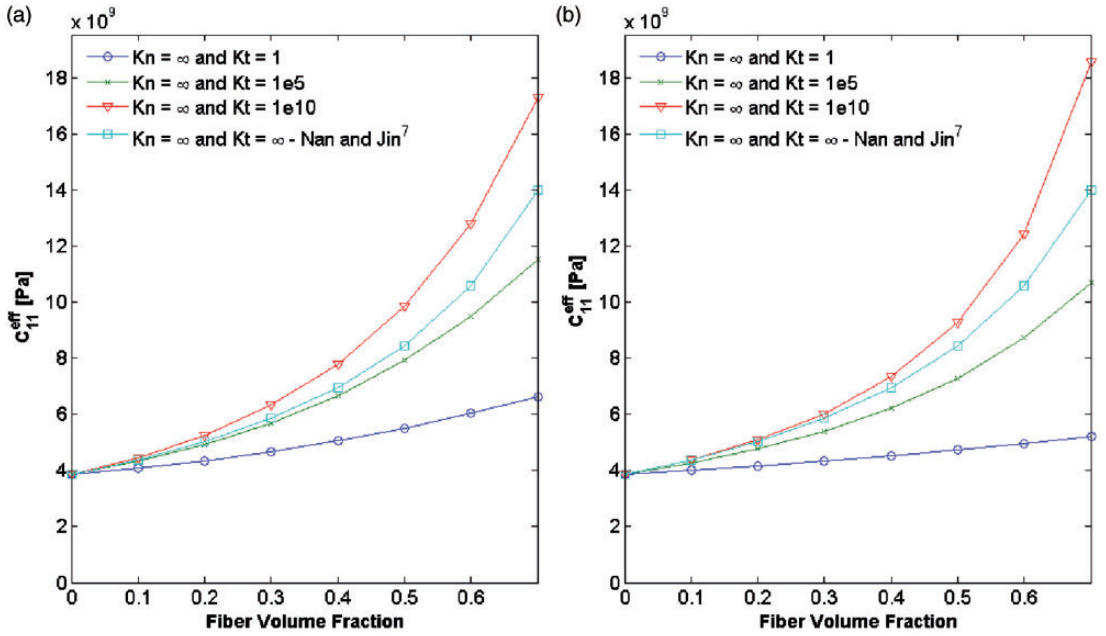

Figure 12. Evolution of elastic property (c_{11}^{eff}) of AFCs as a function of the fiber volume fraction: comparison between the uniform field method and FEA: (a) circular cross section; (b) square cross section.

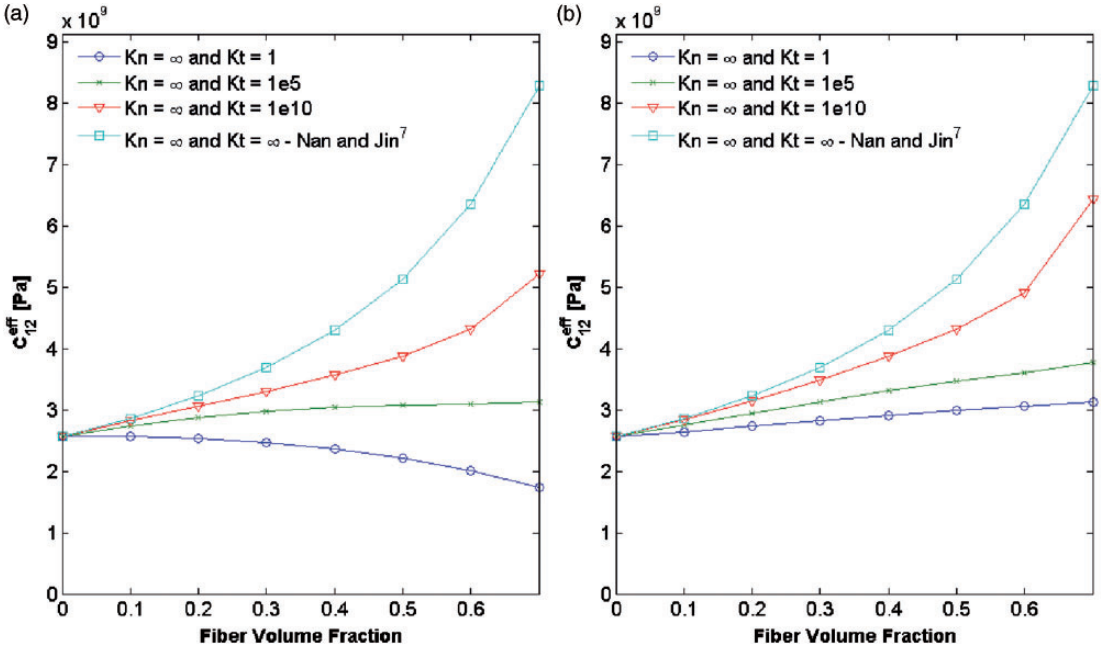

Figure 13. Evolution of elastic property (c_{12}^{eff}) of AFCs as a function of the fiber volume fraction: comparison between the uniform field method and FEA: (a) circular cross section; (b) square cross section.

$mm \times mm^{-2}$) decrease with increasing of the fiber volume fraction, i.e. the composite becomes more flexible. Also, differences between completely imperfect and perfect can be higher than 100%. In fact, this behavior ensures that the parameter K_t influences mainly the transversal effective coefficients.

Regarding the piezoelectric coefficients (Figures 18 to 20), it is possible to observe that the effective coefficient e_{13}^{eff} is strongly influenced by the imperfect contact. The effective coefficient e_{15}^{eff} shows some influence and the coefficient e_{33}^{eff} does not show any influence of the imperfect contact. Thus, the imperfect model presented

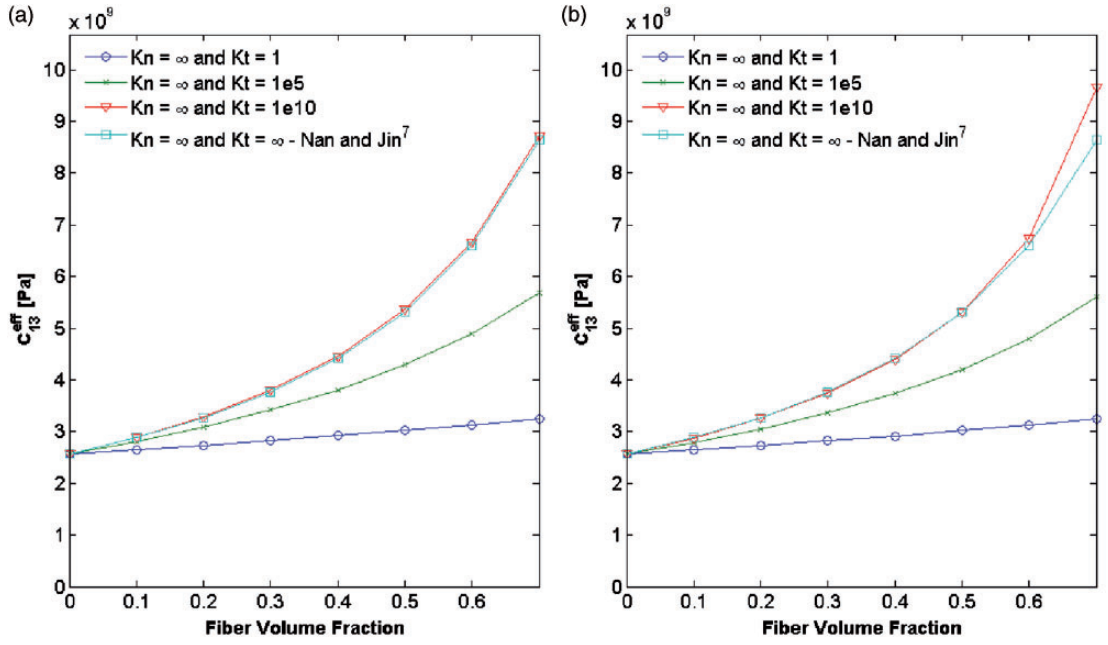

Figure 14. Evolution of elastic property (c_{13}^{eff}) of AFCs as a function of the fiber volume fraction: comparison between the uniform field method and FEA: (a) circular cross section; (b) square cross section.

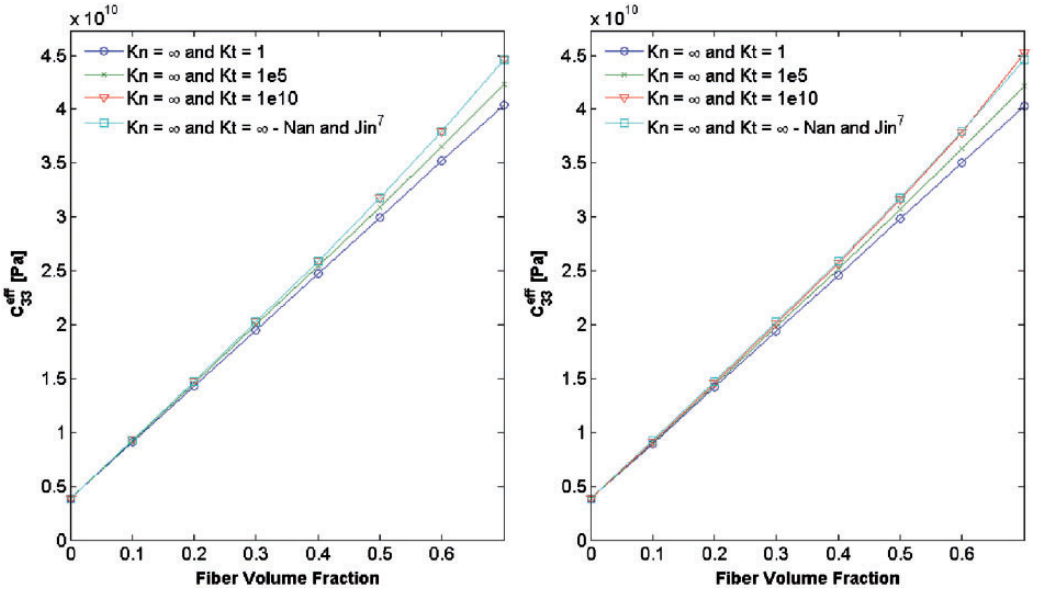

Figure 15. Evolution of elastic property (c_{33}^{eff}) of AFCs as a function of the fiber volume fraction: comparison between the uniform field method and FEA: (a) circular cross section; (b) square cross section.

in this work influences mainly the transversal effective coefficients.

Regarding the dielectric coefficients (Figures 21 and 22), it is possible to conclude that the imperfect condition, as modeled in this work, has no influence in the effective coefficients ε_{11}^{eff} and ε_{33}^{eff}.

As shown by Figures 12 to 22, in general, the effective coefficients for both square and circular fiber cross sections can be very different, considering the level of the imperfect contact as well as the fiber volume fraction. As in previous analyses, the c_{11}^{eff}, c_{12}^{eff}, c_{66}^{eff}, e_{15}^{eff}, and ε_{11}^{eff} coefficients show significant differences for both square and circular fiber cross sections, mainly for fiber volume fractions higher than 30%, due to the aspects previously discussed. Thus, coefficients associated to directions 1 and 2 (transversely direction),

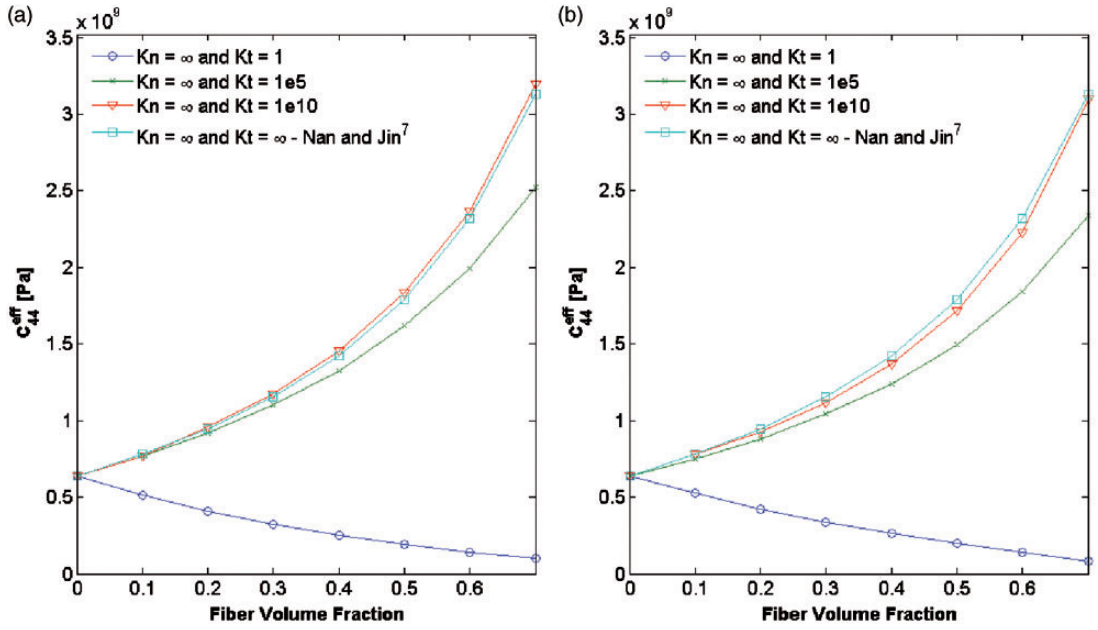

Figure 16. Evolution of elastic property (c_{44}^{eff}) of AFCs as a function of the fiber volume fraction: comparison between the uniform field method and FEA: (a) circular cross section; (b) square cross section.

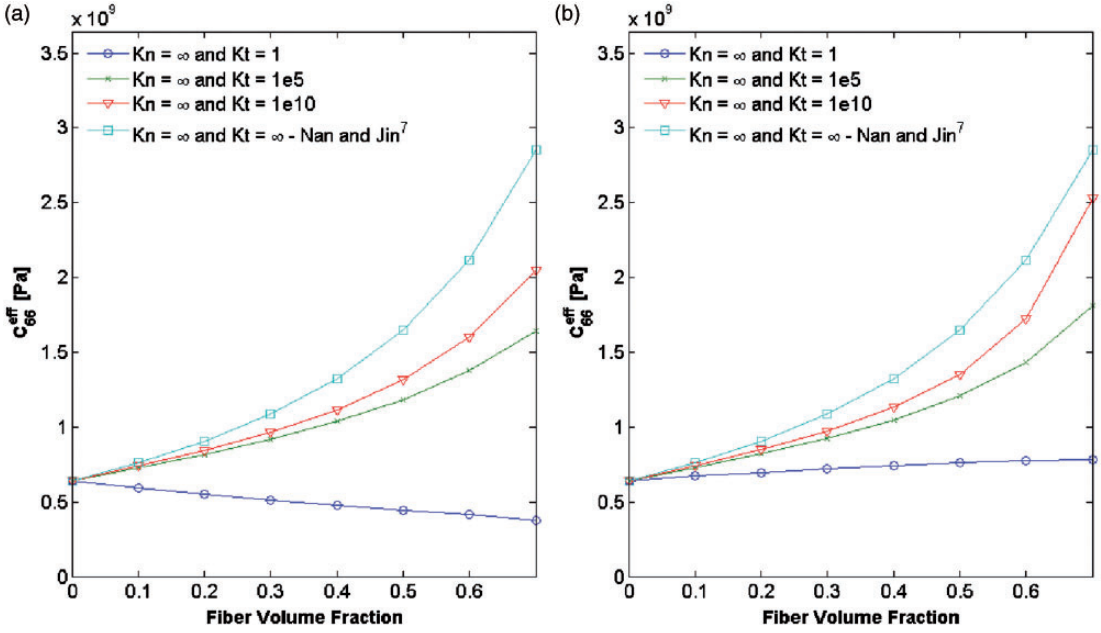

Figure 17. Evolution of elastic property (c_{66}^{eff}) of AFCs as a function of the fiber volume fraction: comparison between the uniform field method and FEA: (a) circular cross section; (b) square cross section.

i.e. transversal the fiber (c_{11}^{eff}, c_{12}^{eff}, and ε_{11}^{eff}), show higher differences.

All effective coefficients, which are oriented in direction 3 (longitudinal direction), i.e. along the fiber (c_{33}^{eff} and ε_{33}^{eff}), show lower differences. This occurs even for a wide range of fiber volume fraction and for different levels of the imperfect contact. In fact, all the coefficients related to direction 3 almost show the same value for different K_t. However, for the coefficients associated to directions 1 and 2, the values decrease in function of increment of imperfections. This behavior is due to the imposed imperfect condition, since the parameter K_t influences mainly the transversal effective coefficients. However, it is possible to

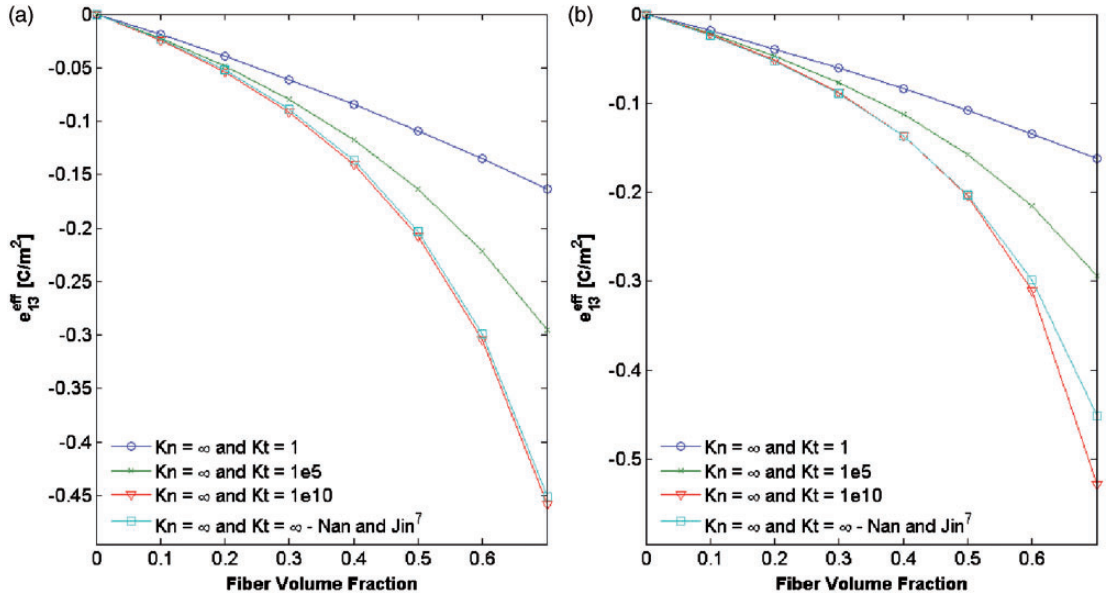

Figure 18. Evolution of piezoelectric property (e_{13}^{eff}) of AFCs as a function of the fiber volume fraction: comparison between the uniform field method and FEA: (a) circular cross section; (b) square cross section.

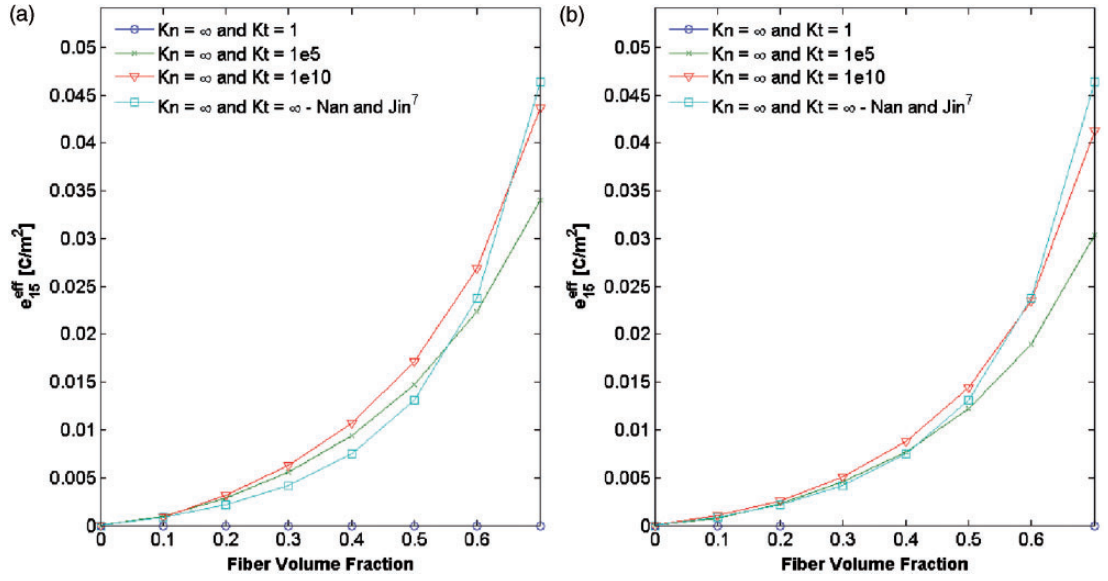

Figure 19. Evolution of piezoelectric property (e_{15}^{eff}) of AFCs as a function of the fiber volume fraction: comparison between the uniform field method and FEA: (a) circular cross section; (b) square cross section.

observe that the imperfect contact model, considering only the degradation of the mechanical properties, not only influence the elastic constants, but also the piezoelectric effective values.

Regarding the comparison between square and circular cross section, it is possible to conclude that the coefficients c_{11}^{eff}, c_{12}^{eff}, c_{66}^{eff}, and e_{15}^{eff} present the higher differences. They can be higher than 51% for K_t equaling 1×10^0 (N/mm $\times$ mm^{-2}). However, these differences decrease with increasing K_t values, showing a maximum difference of 20% for K_t equaling 1×10^{10} (N/mm $\times$ mm^{-2}).

Conclusions

By using the proposed numerical approach, longitudinal and transversal effective coefficients for a PZT fiber embedded in a nonpiezoelectric material (epoxy

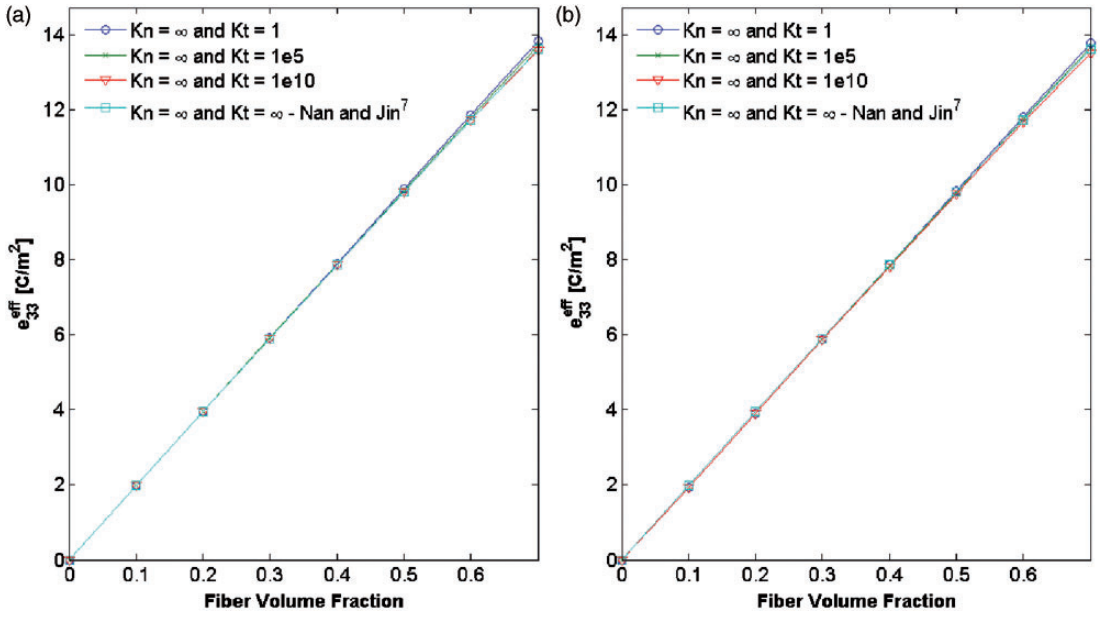

Figure 20. Evolution of piezoelectric property (e_{33}^{eff}) of AFCs as a function of the fiber volume fraction: comparison between the uniform field method and FEA: (a) circular cross section; (b) square cross section.

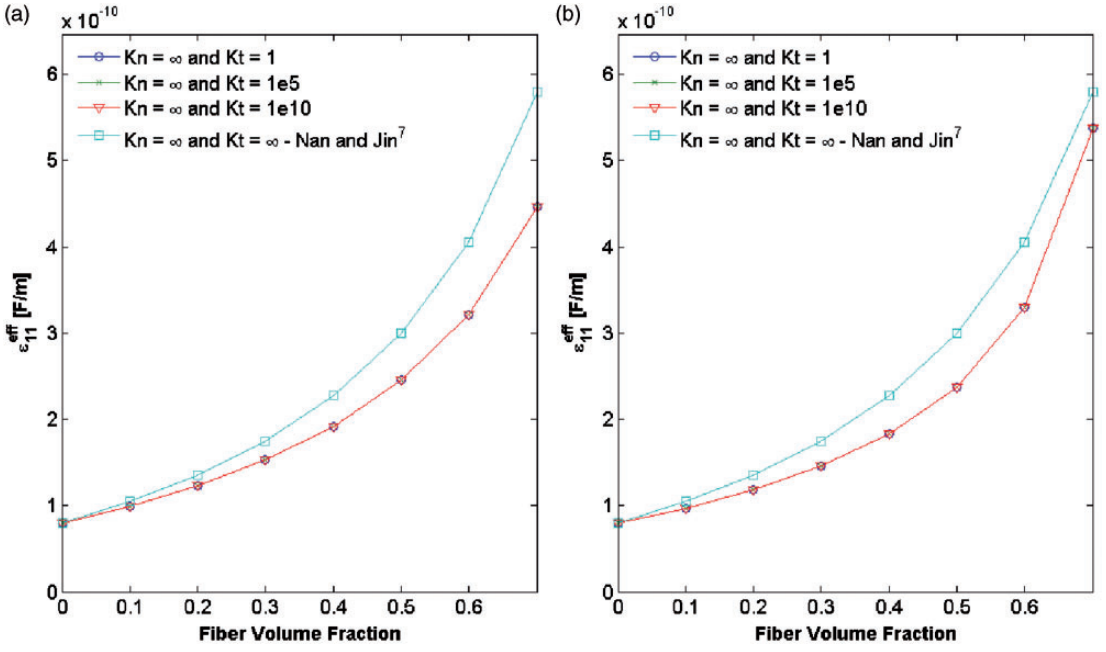

Figure 21. Evolution of dielectric property (ε_{11}^{eff}) of AFCs as a function of the fiber volume fraction: comparison between the uniform field method and FEA: (a) circular cross section; (b) square cross section.

resin matrix) are evaluated and compared to other approaches found in the literature. The proposed approach requires particular care with RVE boundary conditions. If the boundary conditions are not applied correctly, then rigid body motions may occur and contaminate the numerical calculations. Although, great amount of boundary conditions may lead to over constrained RVE, thereby affecting the model performance. Therefore, it is very important to balance the boundary conditions application as shown in the section "Loadings and boundary conditions applied on the RVE models".

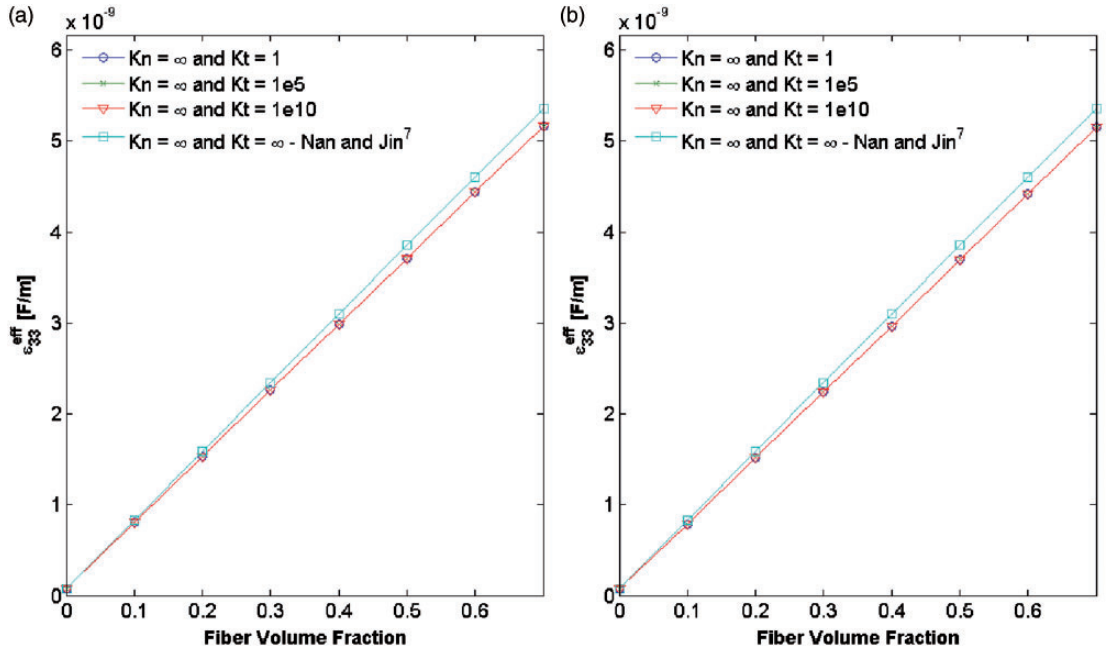

Figure 22. Evolution of dielectric property (ε_{33}^{eff}) of AFCs as a function of the fiber volume fraction: comparison between the uniform field method and FEA: (a) circular cross section; (b) square cross section.

Different case studies were investigated by using the proposed approach in order to evaluate the influence of different parameters on the effective coefficients of smart composite materials. Among these parameters, it is possible to cite: geometry of the fiber cross section, fiber volume fraction and, mainly, the imperfection in the fiber–matrix adhesion. Regarding the square arrangement of fibers with circular geometry and contact perfect, it is concluded that the results are similar to those verified in the literature. Regarding the square arrangement of fibers with square geometry and contact perfect, it is concluded that the effective coefficients calculated via proposed approach satisfy the Universal Relations provided by Benveniste and Dvorak.[6] It is important to notice that the effective values verified using the Universal Relations provided differences less than 0.1%.

It is shown that the effective coefficients for both square and circular fiber cross-sections can be very different, considering the level of the imperfect contact as well as the fiber volume fraction. It is concluded that the coefficients associated to directions 1 and 2 (transversely direction) show higher differences. However, all effective coefficients, which are oriented in direction 3 (longitudinal direction) show lower differences. This occurs even for a wide range of fiber volume fraction and for different levels of the imperfect contact. Indeed, this behavior is due to the imposed imperfect condition, since the parameter K_t influences mainly the transversal effective coefficients. Also, it is possible to conclude that the imperfect contact not only modifies mechanical coefficients of the smart composite material, but also piezoelectric coefficients due to the natural coupling effects.

Finally, as shown, the proposed numerical approach based on RVE and FEA can predict the homogenized properties for piezoelectric fiber composites, mainly considering imperfect fiber–matrix adhesion. Therefore, the present procedure can aid to design smart composite materials. In future works, the authors will investigate this problem, considering different combinations of parameters and values, using functionally graded materials and experimental analysis, as well. Besides, by using the proposed methodology, the authors can investigate others piezoelectric fibers like PZT-7 A as well as others arrangements (e.g. rhombic cell arrangements), and the results can be compared to other researchers.[43–45]

Acknowledgement

The authors are thankful to Prof. Reginaldo Teixeira Coelho (University of Sao Paulo) for kindly permitting the use of the Abaqus™ license.

Funding

The authors acknowledge the financial support of the Sao Paulo State Research Foundation (FAPESP process number: 2012/01047-8 and 2012/03645-0). As well as, Coordination for the Improvement of the Higher Level Personnel (CAPES process number: 011214/2013-09) and National Council for Scientific and Technological Development (CNPq process number: 574001/2008-5) and the FAPEMIG (TEC APQ 00076-09) for partially funding the present research work through the INCT-EIE.

References

1. Hagood NW and Bent AA. Development of piezoelectric fiber composites for structural actuation. *AIIA Paper* 1993; 1717: 3625–3638.
2. Wilkie WK, High WJ, Mirick PH, et al. Low-cost piezocomposite actuator for structural control applications. In: *SPIE's 7th annual international symposium on smart structures and materials,* Newport Beach, CA, USA, 2000.
3. Chan HLW and Unsworth J. Simple model for piezoelectric ceramic/polymer 1-3 composites used in ultrasonic transducer applications. *IEEE Trans Ultrason Ferroelectr Freq Control* 1989; 36: 434–441.
4. Smith WA and Auld BA. Modeling 1-3 composite piezoelectrics: Thickness-mode oscillations. *IEEE Trans Ultrason Ferroelectr Freq Control* 1991; 38: 40–47.
5. Schulgasser K. Relationships between the effective properties of transversely isotropic piezoelectric composites. *J Mech Phys Solids* 1992; 40: 473–479.
6. Benveniste Y and Dvorak GJ. Uniform fields and universal relations in piezoelectric composites. *J Mech Phys Solids* 1992; 40: 1295–1312.
7. Nan CW and Jin FS. Multiple-scattering approach to effective properties of piezoelectric composites. *Phys Rev B* 1993; 48: 8578–8582.
8. Rodríguez-Ramos R, Sabina FJ, Guinovart-Díaz R, et al. Closed-form expressions for the effective coefficients of a fiber reinforced composite with transversely isotropic constituents - I. Elastic and square symmetry. *Mech Mater* 2001; 33: 223–235.
9. Bravo-Castillero J, Guinovart-Díaz R, Sabina FJ, et al. Closed-form expressions for the effective coefficients of a fiber reinforced composite with transversely isotropic constituents - II. Piezoelectric and square symmetry. *Mech Mater* 2001; 33: 237–248.
10. Sevostianov I, Levin V and Kachanov M. On the modeling and design of piezocomposites with prescribed properties. *Arch Appl Mech* 2001; 71: 733–747.
11. Otero JA, Bravo-Castillero J, Guinovart-Diaz R, et al. Analytical expressions of effective constants for a piezoelectric composite reinforced with square cross-section fibers. *Arch Mech* 2003; 55: 357–371.
12. Ray MC. Micromechanics of piezoelectric composites with improved effective piezoelectric constant. *Int J Mech Des* 2006; 3: 361–371.
13. Deraemaeker A, Nasser H, Benjeddou A, et al. Mixing rules for the piezoelectric properties of macro fiber composites. *J Intel Mat Syst Str* 2009; 20: 1475–1482.
14. Kumar A and Chakraborty D. Effective properties of thermo-electro-mechanically coupled piezoelectric fiber reinforced composites. *Mater Des* 2009; 30: 1216–1222.
15. Ghasemi-Nejhad MN, Russ R and Pourjalali S. Manufacturing and testing of active composite panels with embedded piezoelectric sensors and actuators. *J Intel Mat Syst Str* 2005; 16: 319–333.
16. Wickramasinghe VK and Hagood NW. Durability characterization of active fiber composite actuators for helicopter rotor blade applications. *J Aircraft* 2004; 41: 931–937.
17. Wickramasinghe VK and Hagood NW. Material characterization of active fiber composites for integral twist-actuated rotor blade application. *Smart Mater Struct* 2004; 13: 1155–1165.
18. Gaudenzi P. On the electromechanical response of active composite materials with piezoelectric inclusions. *Comput Struct* 1997; 65: 157–168.
19. Berger H, Kari S, Gabbert U, et al. An analytical and numerical approach for calculating effective material coefficients of piezoelectric fiber composites. *Int J Solids Struct* 2005; 42: 5692–5714.
20. Berger H, Kari S, Gabbert U, et al. Unit cell models of piezoelectric fiber composites for numerical and analytical calculation of effective properties. *Smart Mater Struct* 2006; 15: 451–458.
21. Kar-Gupta R and Venkatesh T. Electromechanical response of 1-3 piezoelectric composites: An analytical model. *Acta Mater* 2007; 55: 1093–1108.
22. Paradies R and Melnykowycz M. Numerical stress investigation for piezoelectric elements with a circular cross section and interdigitated electrodes. *J Intel Mat Syst Str* 2007; 18: 963–972.
23. Trindade MA and Benjeddou A. Effective electromechanical coupling coefficients of piezoelectric adaptive structures: Critical evaluation and optimization. *Mech Adv Mater Struct* 2009; 16: 210–223.
24. Medeiros R, Rodríguez-Ramos R, Guinovart-Díaz R, et al. Numerical and analytical analyses for active fiber composite piezoelectric composite materials. *J Intel Mater Syst Struct* 2014; 1045389X14521881.
25. Trindade MA and Benjeddou A. Finite element homogenization technique for the characterization of d_{15} shear piezoelectric macro-fibre composites. *Smart Mater Struct* 2011; 20: 075012.
26. Würkner M, Berger H and Gabbert U. On numerical evaluation of effective material properties for composite structures with rhombic fiber arrangements. *Int J Eng Sci* 2011; 49: 322–332.
27. Medeiros R, Moreno ME, Marques FD, et al. Effective properties evaluation for smart composite materials. *J Braz Soc Mech Sci Eng* 2012; 34: 362–370.
28. Shari H-Z and Chou T-W. Transverse elastic moduli of unidirectional fiber composite with fiber/matrix interfacial debonding. *Compos Sci Technol* 1995; 53: 383–391.
29. Achenbach JD and Zhu H. Effect of interfacial zone on mechanical behavior and failure of fiber-reinforced composites. *J Mech Phys Solids* 1989; 37: 381–393.
30. Hashin Z. The spherical inclusion with imperfect interface. *J Appl Mech* 1991; 58: 444–453.
31. Hashin Z. Thermoelastic properties of particulate composites with imperfect interface. *J Mech Phys Solids* 1991; 39: 745–762.
32. Hashin Z. Thin interphase/imperfect interface in elasticity with application to coated fiber composites. *J Mech Phys Solids* 2002; 50: 2509–2537.
33. Caporale A, Luciano R and Sacco E. Micromechanical analysis of interfacial debonding in unidirectional fiber-reinforced composites. *Comput Struct* 2006; 84: 2200–2211.

34. Rodríguez-Ramos R, Guinovart-Díaz R, Lópes-Realpozo JC, et al. Influence of imperfect elastic contact condition on the antiplane effective properties of piezoelectric fibrous composites. *Arch Appl Mech* 2010; 80: 377–388.
35. Lópes-Realpozo JC, Rodríguez-Ramos R, Guinovart-Díaz R, et al. Transport properties in fibrous elastic rhombic composite with imperfect contact condition. *Int J Mech Sci* 2011; 53: 98–107.
36. Sabina FJ, Guinovart-Díaz R, Rodríguez-Ramos R, et al. Overall properties in fibrous elastic composite with imperfect contact condition. *Int J Eng Sci* 2012; 61: 142–155.
37. Xu Y, Du S, Xiao J, et al. Evaluation of the effective elastic properties of long fiber reinforced composites with interphases. *Comput Mater Sci* 2012; 61: 34–41.
38. Rodríguez-Ramos R, Medeiros R, Guinovart-Díaz R, et al. Different approaches for calculating the effective elastic properties in composite materials under imperfect contact adherence. *Compos Struct* 2013; 99: 264–275.
39. Jin KK, Huang Y, Lee YH, et al. Distribution of micro stresses and interfacial tractions in unidirectional composites. *J Compos Mater* 2008; 42: 1825–1849.
40. Xia Z, Zhang Y and Ellyin F. A unified periodical boundary conditions for representative volume elements of composites and applications. *Int J Solids Struct* 2003; 40: 1907–1921.
41. Guinovart-Diaz R, Rodriguez-Ramos R, Bravo-Castillero J, et al. Modeling of three-phase fibrous composite using the asymptotic homogenization method. *Mech Adv Mater Struct* 2003; 10: 1–15.
42. Abaqus. *Version 6.10 documentation*. Pawtucket, RI: Hibbitt, Karlsson & Sorensen, 2010.
43. Rodriguez-Ramos R, Guinovart-Diaz R, Lopez-Realpozo JC, et al. Effective properties of periodic fibrous electro-elastic composites with mechanic imperfect contact condition. *Int J Mech Sci* 2013; 73: 1–13.
44. Guinovart-Díaz R, Rodríguez-Ramos R, Bravo-Castillero J, et al. Electro-mechanical moduli of three-phase fiber composites. *Mater Lett* 2008; 62: 2385–2387.
45. Würkner M, Berger H and Gabbert U. Numerical study of effective elastic properties of fiber reinforced composites with rhombic cell arrangements and imperfect. *Int J Eng Sci* 2013; 63: 1–9.